



3 Model of spills and fires from LNG and oil tankers

5 J.A. Fay*

6 *Department of Mechanical Engineering, Massachusetts Institute of Technology, Cambridge, MA 02139, USA*

7 Received 30 March 2002; received in revised form 1 April 2002; accepted 3 June 2002

8 Abstract

9 A comprehensive model for predicting the dynamics of spills from LNG and oil product tankers
10 is constructed from fluid mechanics principles and empirical properties of oil and LNG spills on
11 water. The analysis utilizes the significant tanker hold and discharge flow area dimensions to specify
12 the cargo liquid outflow history and the ensuing pool characteristics, including the establishment
13 of a pool fire. The pool fire area, duration, and heat release rate are determined as functions of the
14 tanker cargo variables. Examples of an LNG and gasoline spill show that for likely discharge flow
15 areas these spills may be regarded as instantaneous, simplifying the evaluation of risk consequences.
16 © 2002 Published by Elsevier Science B.V.

17 *Keywords:* LNG; Pool fire; Tanker spills; Oil products; Spill model; Underwater spill

18 1. Introduction

19 The great increase in oceanic shipping of crude oil in large supertankers following World
20 War II, and the subsequent occasional accidental episodes of disastrous oil spills from these
21 vessels that harmed coastal environments, led to development of models for the spread
22 of oil spills on the surface of the sea [1] and corroborating laboratory measurements [2].
23 These models confirmed the common observation that significant spills spread rapidly to
24 encompass large areas of the ocean surface, well beyond the capacity to contain them by
25 mechanical means within the short time of spreading.

26 In the 1970s, the development of oceanic tankers transporting cryogenic liquids (LNG,
27 LPG, ethylene) posed additional spill risks of combustion, either at the spill site or at
28 downwind locations to which the spill vapors might travel [3,4]. In the intervening years,
29 a considerable amount of theoretical and experimental research has been conducted on
30 the evaporation of cryogenic spills on land and water, the dispersion and combustion of

* Tel.: +1-617-253-2236; fax: +1-617-258-8559.
E-mail address: jfay@mit.edu (J.A. Fay).

31 the evolved vapor clouds, and the establishment of pool fires at the spill site (for a recent
32 summary, see [5]).

33 In siting and licensing marine terminals where LNG is landed from tankers, public au-
34 thorities have had to consider the possibility of accidental spills, usually considered to be a
35 consequence of a ship collision or grounding. But the recent episodes of bombing incidents,
36 including the attack in 2000 on the USS Cole, have raised the issue of other sources of vessel
37 damage that might result in spills that form pool fires alongside the stricken vessel.

38 Raj and Kalelkar [6] and Raj [7] have considered the formation of an LNG pool fire
39 from a spill of given volume delivered to a level surface (either water or land) at a uniform
40 rate over a given time period. In the limit of very short time, the spill may be considered
41 instantaneous and the resulting pool fire spreads to a size and burns at a rate determined by
42 the spill volume and the LNG fuel properties. In the alternate limit of a long period of spill
43 discharge, the pool fire characteristics are determined by the volumetric discharge rate. In
44 either case, the spill volume and discharge time are exogenous variables determining the
45 pool fire characteristics.

46 The spill volume, discharge rate, and duration are significant determinants of the spill
47 behavior. For a spill from a ocean tanker, these are dependent upon the tanker hold size
48 and configuration, the size and location of the vessel's rupture opening, and of course, the
49 properties of the cargo fluid. This paper models both the discharge process and the pool
50 spread behavior, expressing the significant results (pool area, pool fire duration, heat release
51 rate) in terms of the tanker hold and rupture variables, covering the entire practical range.
52 Examples are given for spills from typical LNG and oil product tankers.

53 2. Fluid mechanics of the spill process

54 Liquid hydrocarbon fuel tankers carry cargo that is less dense than sea water. The re-
55 quirements for hull strength and reserve buoyancy result in cargo tanks in which the top
56 surface of the liquid cargo is elevated above that of the surrounding sea water, to an extent
57 that creates a liquid hydrostatic pressure within the cargo tank exceeding that of the sur-
58 rounding atmosphere or sea water at the same elevation. Any puncture of the vessel's side
59 walls permits the cargo to flow out to the surrounding environment at a velocity determined
60 by the pressure difference between the cargo and the exterior atmosphere or sea water at
61 the level of the puncture opening.

62 The emerging hydrocarbon cargo fluid, being immiscible with and less dense than sea
63 water, floats on the sea water surface. It forms a pool, centered at the rupture site, that spreads
64 horizontally, induced by a horizontal pressure gradient resulting from the gravitational force
65 on the liquid layer. For the very large spill rates being considered here, the spreading rate
66 is governed by a balance between fluid inertia and the gravity force, called gravity-inertia
67 spread [1]. Although the spreading of the pool is enhanced by the flow of liquid from the
68 cargo tank, it nevertheless continues as long as there is a finite volume of liquid in the pool.

69 The pool fluid can be vaporized by two processes. If it is a cryogenic fluid, such as liquified
70 natural gas, propane, or ethylene, having a boiling point below the sea water temperature, it
71 will boil vigorously by virtue of its contact with the underlying sea water. If vapor evolving
72 from the pool catches fire, establishing a pool fire above the spreading liquid fuel, thermal

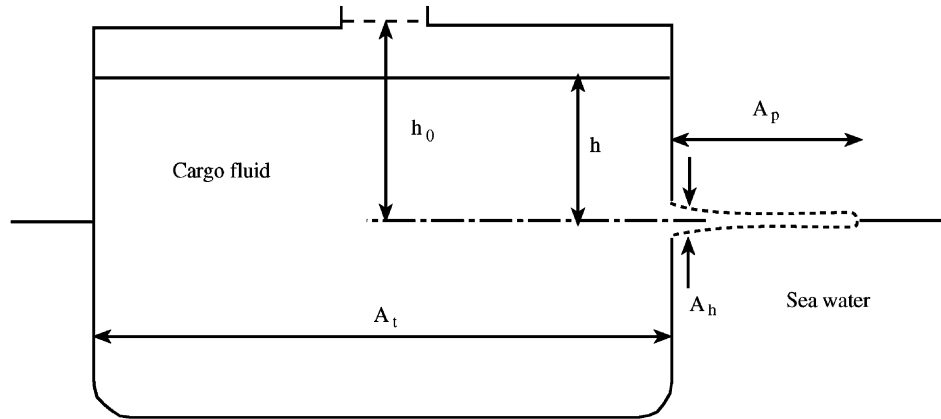


Fig. 1. A sketch of the cross-section of a tanker vessel, showing the configuration of the cargo fluid in a tanker during outflow through a rupture in the side of the vessel.

73 radiation from the pool fire will heat and vaporize the liquid fuel. In the case of pool fires
 74 above cryogenic fuel spills, both processes act in parallel to increase the rate of vaporization.

75 The configuration of the cargo fluid in a tanker hold during its flow out through a rupture
 76 at the level of the waterline is sketched in Fig. 1. The rupture flow area is denoted by A_h ,
 77 while the upper surface area of the cargo fluid is A_t . The time-varying hydrostatic head h
 78 governing the fluid velocity through the rupture is, in this case, the vertical distance from
 79 the rupture centerline to the free surface of the cargo fluid. The lateral area of the liquid
 80 pool outside the vessel, A_p , is a function of time, depending upon the spreading of the cargo
 81 fluid that leaks from the tank.

82 There is a time scale t_d that characterizes the duration of the outflow from the ruptured
 83 cargo tank. The magnitude of the outflow velocity through the rupture is $\sqrt{gh_0}$, so that the
 84 outflow volume flow rate $\sqrt{gh_0}A_h$ times the discharge time t_d must equal the volume $A_t h_0$
 85 discharged (where h_0 is the initial value of h), giving

$$86 \quad t_d \sim \frac{A_t h_0}{\sqrt{gh_0} A_h} = \frac{A_t}{A_h} \sqrt{\frac{h_0}{g}} \quad (1)$$

87 Whether the liquid pool formed from this discharge is vaporized by boiling or the estab-
 88 lishment of a pool fire, it cannot be depleted in a time shorter than t_d .

89 The rate of loss of the pool liquid by vaporization may be characterized by a regression
 90 velocity w , where the volume rate of pool liquid vaporized per unit surface area is w . The
 91 regression velocity is a function of the processes that evaporate the fluid, boiling and/or pool
 92 fire heating, and the fluid properties. It is this regression velocity which limits the maximum
 93 size of the pool area, which would otherwise continue to increase indefinitely [1].

94 We can distinguish two limiting cases of pool size. If the rupture area A_h is very small,
 95 a quasi-steady pool evaporation process will be established, for which the evaporation rate
 96 from the pool will equal the discharge rate from the vessel. In this case, the lifetime of
 97 the pool formation and extinction will equal the discharge duration t_d . Alternatively, if the

98 rupture area A_h is very large, the pool will spread as if from an instantaneous discharge and
 99 will persist for a much longer time than t_d in order to vaporize all the discharged volume.

100 The maximum pool area for the case of small A_h may be found by equating the discharge
 101 volume flow rate $\sqrt{gh_0}A_h$ to the vaporization rate wA_p , giving

$$102 \quad A_p \sim \frac{\sqrt{gh_0}A_h}{w} \quad (2)$$

103 Because w is always quite small compared to $\sqrt{gh_0}$ for practical cases, the pool area is large
 104 compared with the rupture area.

105 Estimating the corresponding evaporation time and pool area for the case of large rupture
 106 area is complicated by the dynamics of the pool spreading. For the latter, the pool area A_p
 107 resulting from an instantaneous spill of volume $A_t h_0$, after a time t_v , is approximately [1,3]

$$108 \quad A_p \sim (\sqrt{g\Delta(A_t h_0)})t_v \quad (3)$$

109 where

$$110 \quad \Delta \equiv \frac{\rho_w - \rho_f}{\rho_w} \quad (4)$$

111 ρ_w and ρ_f being the sea water and cargo fluid mass densities, respectively. Setting the
 112 evaporation loss from the pool during the time t_v equal to the cargo spill volume,

$$113 \quad A_p w t_v \sim h_0 A_t \quad (5)$$

114 we can solve Eqs. (3) and (5) for the evaporation time and pool area at that time:

$$115 \quad t_v \sim \frac{(A_t h_0)^{1/4}}{w^{1/2}(g\Delta)^{1/4}} \quad (6)$$

$$116 \quad A_p \sim \frac{(A_t h_0)^{3/4}(g\Delta)^{1/4}}{w^{1/2}} \quad (7)$$

117 We may now contrast the behavior of the pool formation and ultimate disappearance for
 118 small and large A_h . For small A_h , the pool area is a maximum at the beginning of the
 119 spill, declining in size in proportion to the outflow rate and disappearing at the discharge
 120 duration given in (1). The maximum pool area is proportional to A_h (see (2)), and the pool
 121 evaporation time is inversely proportional to A_h (see (1)). In contrast, for very large A_h , the
 122 pool size grows during the outflow process, reaching a maximum size at the end of the pool
 123 evaporative lifetime (6) as given in Eq. (7). In this case, both the evaporative time and the
 124 maximum pool size are independent of the hole size A_h , provided it is large enough. But
 125 both the small and large A_h approximations give equal values for A_p and t_v when A_h is:

$$126 \quad A_h \sim A_t^{3/4} w^{1/2} \Delta^{1/4} \left(\frac{h_0}{g}\right)^{1/4} \quad (8)$$

127 It is this value of A_h that determines whether A_h is small or large. It will be seen below that
 128 the ratio of the two sides of (8) is a parameter in an exact description of the pool behavior.

129 2.1. Analytical model

130 To develop a more accurate model of the spill and pool behavior, we begin by considering
 131 the outflow through the puncture area A_h . Equating the rate of loss of cargo volume to the
 132 outflow volumetric flow rate,

$$133 \quad -\left(\frac{d(hA_t)}{dt}\right) = \sqrt{2gh}A_h \quad (9)$$

134 we obtain, by integration,

$$135 \quad h = \begin{cases} \left(\sqrt{h_0} - \sqrt{\frac{g}{2}} \frac{A_h}{A_t} t\right)^2, & \text{if } 0 \leq t \leq \sqrt{\frac{2h_0}{g}} \left(\frac{A_t}{A_h}\right) \\ 0, & \text{if } t \geq \sqrt{\frac{2h_0}{g}} \left(\frac{A_t}{A_h}\right) \end{cases} \quad (10)$$

136 We next determine the rate of change of volume V_p of the fluid in the pool, as a consequence
 137 of the inflow from the rupture minus the evaporation from the pool area A_p :

$$138 \quad \frac{dV_p}{dt} = \sqrt{2gh}A_h - wA_p \quad (11)$$

139 We now express the spreading rate of the pool, which is assumed to be semicircular in
 140 shape, of radius R and area $A_p = \pi R^2/2$, in the form given in [3]:

$$141 \quad \frac{dR}{dt} = \beta \left(g\Delta \frac{V_p}{\pi R^2/2}\right)^{1/2} \quad (12)$$

142 where β is an empirical constant and the factor $V_p/(\pi R^2/2)$ is the average thickness of the
 143 pool. This may be transformed to the form:

$$144 \quad \frac{dA_p}{dt} = \frac{d(\pi R^2/2)}{dt} = \beta \sqrt{2\pi g\Delta V_p} \quad (13)$$

145 defining the time rate of growth of the pool area.

146 Eqs. (10), (11) and (13) define the time history of the outflow from the vessel and the
 147 subsequent pool formation and vaporization. As described in Section 2, the nature of this
 148 history depends critically on the size of A_h through its relationship to other parameters
 149 of the flow. To proceed to elucidate and simplify this relationship, it is useful to express
 150 these equations in dimensionless form. To this end we choose the following dimensionless
 151 variables:

$$152 \quad t^* \equiv \left(\frac{A_h}{A_t}\right) \sqrt{\frac{g}{h_0}} t, \quad v^* \equiv \frac{V_p}{h_0 A_t}, \quad a^* \equiv \frac{wA_p}{A_h \sqrt{gh_0}}, \quad h^* \equiv \frac{h}{h_0} \quad (14)$$

153 Here we have introduced time, volume, area, and length scales $(\sqrt{h_0/g}A_t)/A_h$, $h_0 A_t$,
 154 $A_h \sqrt{gh_0}/w$, and h_0 to define the dimensionless variables. Eqs. (10), (11) and (13) then

155 assume the form:

$$156 \quad h^* = \begin{cases} \left(1 - \frac{t^*}{\sqrt{2}}\right)^2, & 0 \leq t^* \leq \sqrt{2} \\ 0, & t^* \geq \sqrt{2} \end{cases} \quad (15)$$

$$157 \quad \frac{dv^*}{dt^*} = \sqrt{2h^*} - a^* \quad (16)$$

$$158 \quad \frac{da^*}{dt^*} = \phi\sqrt{v^*} \quad (17)$$

159 where the parameter ϕ has the value

$$160 \quad \phi \equiv \beta\sqrt{2\pi\Delta w} \sqrt{\frac{h_0}{g} \frac{A_t^{3/2}}{A_h^2}} \quad (18)$$

161 By comparison with (8), we now see that $\phi \gg 1$ corresponds to small A_h while $\phi \ll 1$
162 defines the case of large A_h .

163 Before proceeding to discuss the solutions for particular values of ϕ , we develop a general
164 relation for the time-averaged value of a^* , denoted by \bar{a}^* . Integrating (15) and (16) over the
165 time interval ($t_v^* \geq \sqrt{2}$) for the pool to evaporate, we find

$$166 \quad \bar{a}^* = \frac{1}{t_v^*} \quad (19)$$

167 This relationship expresses the conservation of mass; all of the cargo fluid drained from the
168 ship's hold is evaporated from the fluid pool by the end of the evaporation period t_v^* .

169 2.1.1. $\phi \gg 1$

170 In this case, after a short period of time $t_s^* \ll \sqrt{2}$ of unsteady flow, a quasi-steady flow
171 will be established during which the inflow to the pool is balanced by evaporation. This
172 balance is expressed by setting the right side of (16) equal to zero, giving a^* as a function
173 of time:

$$174 \quad a^* = \sqrt{2} - t^*, \quad t_s^* \leq t^* \leq \sqrt{2} \quad (20)$$

175 During this time, the pool area shrinks linearly with time, reaching zero at the end of the
176 discharge, when $t^* = \sqrt{2}$. The pool area at the beginning of the quasi-steady flow, a_s^* ,
177 becomes

$$178 \quad a_s^* = \sqrt{2} - t_s^* \quad (21)$$

179 We next consider the transient flow time period $0 \leq t^* \leq t_s^*$, for which $t^* \ll \sqrt{2}$ and
180 $h^* = 1$. Eq. (16) becomes

$$181 \quad \frac{dv^*}{dt^*} = \sqrt{2} - a^* \quad (22)$$

182 This may be solved simultaneously with (17) to determine v^* as a function of a^* :

$$183 \quad v^* = \left[\frac{3a^*}{2\phi} \left(\sqrt{2} - \frac{a^*}{2} \right) \right]^{2/3} \quad (23)$$

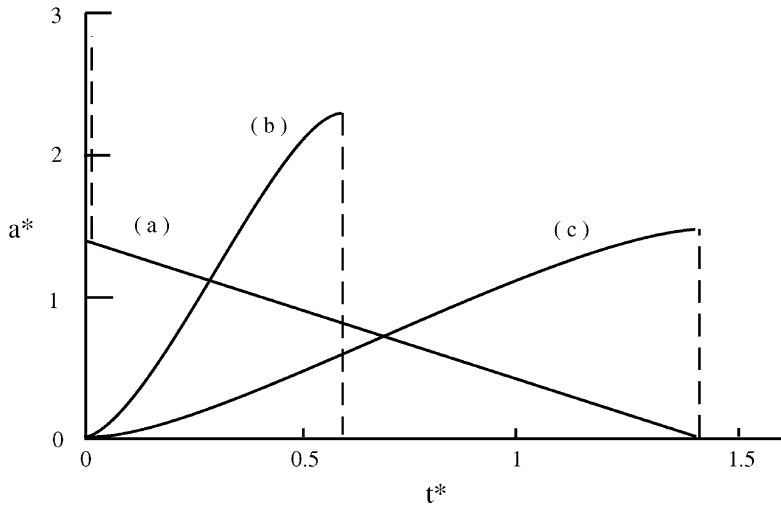


Fig. 2. The dependence of pool area a^* on time t^* for large values of the flow parameter ϕ : (a) $\phi \rightarrow \infty$; (b) $\phi = 10$; (c) $\phi = \phi_c = 1.784$.

184 The pool volume increases during this period, reaching a maximum when $a^* = \sqrt{2}$ and
 185 then decreasing to zero when a^* reaches its maximum value, a_m^* , of

186
$$a_m^* = 2\sqrt{2} \quad (24)$$

187 Note that $a_m^* \geq \sqrt{2}a_s^*$; the transient phase leaves a larger pool than that at the beginning
 188 of the quasi-steady phase. The duration of the transient flow may be found by substituting
 189 (23) in (17):

191
$$t_s^* = \phi^{-2/3} \int_0^{2\sqrt{2}} \frac{da^*}{[3a^*/2(\sqrt{2} - a^*/2)]^{1/3}}$$

 192
$$= \left(2^{7/6} (3^{2/3}) \frac{(\Gamma\{4/3\})^2}{\Gamma\{5/3\}} \right) \phi^{-2/3} = 4.124\phi^{-2/3} \quad (25)$$

193 where $\Gamma\{x\}$ is the gamma function of argument x .

194 For $\phi \rightarrow \infty$, the transient phase is negligible in duration, and the quasi-steady flow
 195 occupies all but the very beginning of the outflow. The dependence of area a^* on time t^*
 196 for this case is shown in Fig. 2(a).

197 In cases where ϕ is not sufficiently large to satisfy the requirement that $t_s^* \ll \sqrt{2}$,
 198 Eqs. (15)–(17) must be integrated numerically. An example is shown in Fig. 2(b) for $\phi =$
 199 10. Here the transient phase is extended to $t_s^* = 0.588$, where $a_m^* = 2.233$ and $a_s^* = 0.827$,
 200 both lower than the values of $2\sqrt{2}$ and $\sqrt{2}$, respectively for $\phi \rightarrow \infty$. Note that a^* varies ap-
 201 proximately linearly with t^* in the transient phase, and exactly so in the quasi-steady phase.

202 For even lower values of ϕ , the transient phase time t_s^* increases while a_m^* and a_s^* decrease,
 203 until at a critical value of $\phi_c = 1.784$, $t_s^* = \sqrt{2}$ and the transient phase occupies the whole
 204 of the outflow duration. For this example, shown in Fig. 2(c), $a_m^* = 1.431$ at $t_v^* = \sqrt{2}$.

205 2.1.2. $\phi \ll 1$

206 In this limit, the discharge occurs quickly, then the pool spreads and evaporates. Focusing
 207 first on the short discharge period where $0 \leq t^* \leq \sqrt{2}$, we may neglect the evaporation
 208 term in (16) and find by integration the time dependence of v^* :

$$209 \quad v^* = \sqrt{2}t^* \left(1 - \frac{t^*}{2\sqrt{2}}\right), \quad t^* \leq \sqrt{2} \quad (26)$$

210 Combining this with (17) and integrating over the discharge period, we find the pool area
 211 a_d^* at $t^* = \sqrt{2}$ to be

$$212 \quad a_d^* = 2^{1/4}\phi \int_0^{\sqrt{2}} \left(t^* \left[1 - \frac{t^*}{2\sqrt{2}}\right]\right)^{1/2} dt^* = \frac{\pi}{2\sqrt{2}}\phi \quad (27)$$

213 For subsequent times where $t^* \geq \sqrt{2}$, Eqs. (16) and (17) then have the form

$$214 \quad \frac{dv^*}{dt^*} = -a^* \quad (28)$$

$$215 \quad \frac{da^*}{dt^*} = \phi\sqrt{v^*} \quad (29)$$

216 with the initial conditions at $t^* = \sqrt{2}$ that $v^* = 1$ and $a^* = a_d^*$, as determined above.
 217 Integrating, we find the variation of v^* with a^* :

$$218 \quad v^* = \left(1 - \frac{3}{4\phi}[(a^*)^2 - (a_d^*)^2]\right)^{2/3} \quad (30)$$

219 The maximum pool area a_m^* occurs when $v^* = 0$:

$$220 \quad (a_m^*)^2 = \frac{4\phi}{3} + \left(\frac{\pi\phi}{2\sqrt{2}}\right)^2$$

$$221 \quad a_m^* \simeq \left(\frac{4\phi}{3}\right)^{1/2} \left[1 + \frac{3\pi^2}{64}\phi\right] = 0.971\phi^{1/2}(1 + 0.463\phi) \quad (31)$$

222 The time t_v^* required to evaporate the pool may be found by combining (31) with (29) and
 223 integrating,

$$224 \quad \int_{\sqrt{2}}^{t_v^*} dt^* = \frac{1}{\phi} \int_{a_d^*}^{a_m^*} \frac{da^*}{\sqrt{v^*}}$$

$$225 \quad t_v^* = \frac{\sqrt{3\pi}}{2} \frac{\Gamma\{5/3\}}{\Gamma\{7/6\}} \phi^{-1/2} + \sqrt{2} - \frac{\pi}{2\sqrt{2}} = 1.493\phi^{-1/2} + 0.304 \quad (32)$$

226 To find a^* as a function of time, one must integrate (28) and (29). For the limit of $\phi \rightarrow 0$,
 227 this integration is shown in Fig. 3(a), using modified coordinates of $a^*/\sqrt{\phi}$ versus $t^*\sqrt{\phi}$.
 228 As expected, the pool area increases with time until evaporation cease at $t^*\sqrt{\phi} = 1.493$
 229 where $a^*/\sqrt{\phi} = 1.155$ (see Eqs. (31) and (32)).

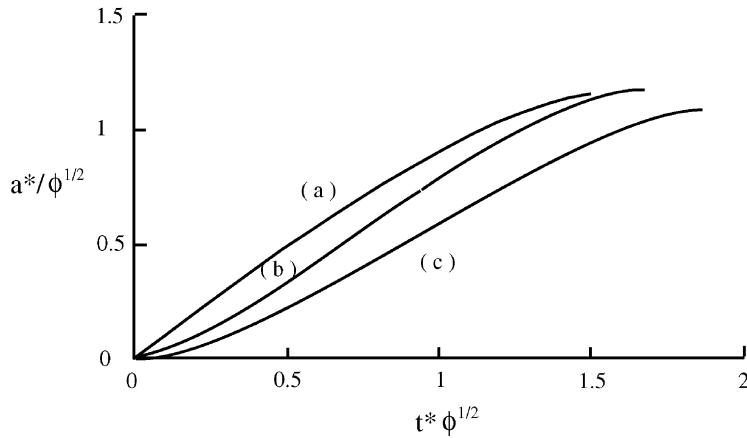


Fig. 3. The dependence of modified pool area $a^*/\sqrt{\phi}$ on modified time $t^*\sqrt{\phi}$ for $\phi \leq \phi_c$: (a) $\phi \rightarrow 0$; (b) $\phi = 1/3$; (c) $\phi = \phi_c = 1.784$.

230 2.1.3. $\phi \leq \phi_c$

231 In general, for values of ϕ in the range $\phi \leq \phi_c$ that are not small enough that the approx-
 232 imations given above are valid, one must resort to numerical integration of Eqs. (15)–(17)
 233 to find the time dependencies of v^* and a^* on t^* and the values of a_m^* and t_v^* . This has been
 234 done for the intermediate case of $\phi = 1/3$ and the limiting value of ϕ_c , and are shown in
 235 Fig. 3(b) and (c), using modified coordinates.

236 2.1.4. Summary

237 The results of the analyses in Sections 2.1.1–2.1.3 above are summarized in Table 1, which
 238 lists the values of a_m^* , t_s^* , a_s^* , t_v^* , and $a_m^*t_v^*$, for eight values of ϕ in the range $0 < \phi < \infty$.
 239 Considered as functions of ϕ , a_m^* increases, while t_v^* decreases, over the range $0 < \phi < \infty$,
 240 reaching the limits of $2\sqrt{2}$ and $\sqrt{2}$, respectively, at $\phi \rightarrow \infty$. Their product, $a_m^*t_v^*$, varies
 241 little over this entire range, reflecting the fact that $\overline{a^*t_v^*} = 1$ is independent of ϕ (see (19)).
 242 We note that the ratio $a_m^*/\overline{a^*}$ lies in the range of 1.724–4.

243 The data of Table 1 for a_m^* and t_v^* as functions of ϕ are plotted in Figs. 4 and 5, respectively,
 244 using logarithmic coordinates. The analytical expressions for $\phi \ll 1$ and $\phi \gg 1$ are shown

Table 1
Pool area and evaporation time

	ϕ							
	$\ll 1$	1/3	1	1.784	3	10	30	$\gg 1$
a_m^*	$1.155\sqrt{\phi}(1 + 0.463\phi)$	0.661	1.113	1.431	1.716	2.233	2.521	2.828
t_s^*				1.414	1.113	0.588	0.300	$4.124\phi^{-2/3}$
a_s^*				0	0.302	0.827	1.114	$(1.414 - 4.124)\phi^{-2/3}$
t_v^*	$1.493/(\sqrt{\phi} + 0.304)$	2.875	1.775	1.414	1.414	1.414	1.414	1.414
$a_m^*t_v^*$	$1.724 + 0.351\sqrt{\phi}$	1.899	1.976	2.024	2.427	3.157	3.565	4.000

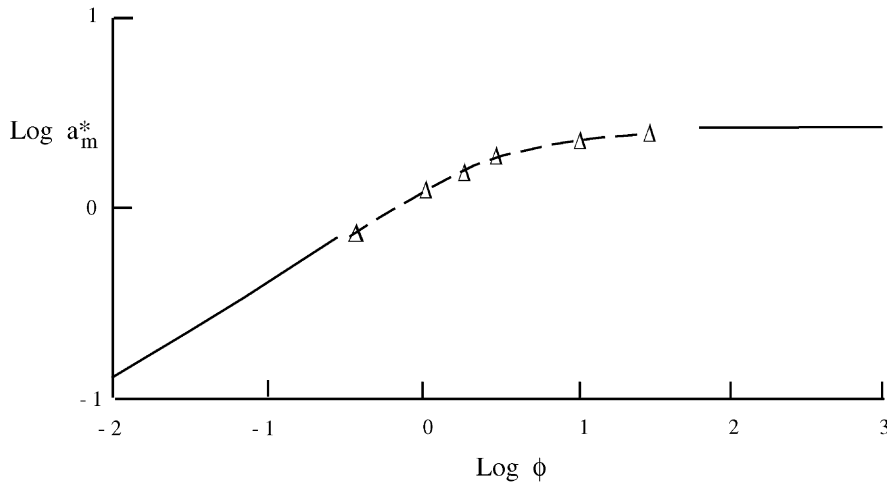


Fig. 4. A plot of the variation of dimensionless maximum pool area a_m^* as a function of the relative outflow parameter ϕ . Data is taken from Table 1.

245 as solid lines while the numerical values are represented by the symbol Δ . These latter are
 246 connected by a faired dashed line. While the transition from one limit to the other occupies
 247 a 100-fold increase in ϕ , this translates into a 10-fold increase in A_h .

248 Values of small A_h (large ϕ) define the region where quasi-steady flow occurs, but in
 249 which there exists some unsteady pool formation. Elsewhere, the pool formation is entirely
 250 unsteady.

251 As mentioned in Section 1, Raj and Kalelkar [6] (see also [8]), have provided solutions
 252 that are equivalent to the two limiting cases of Table 1, $\phi \ll 1$ and $\phi \gg 1$. Expressed
 253 in terms of the a^* and t^* dimensionless variables, their values for $\phi \gg 1$ are identical
 254 to those of a_s^* and t_s^* in Table 1. But for the case of $\phi \ll 1$, they find $a_m^* = 1.56\phi^{1/2}$,
 255 $t_v^* = 1.355\phi^{-1/2}$, $a_m^*t_v^* = 2.118$, and $\bar{a}t_v^* = 1$. The first two of these are 35% higher and

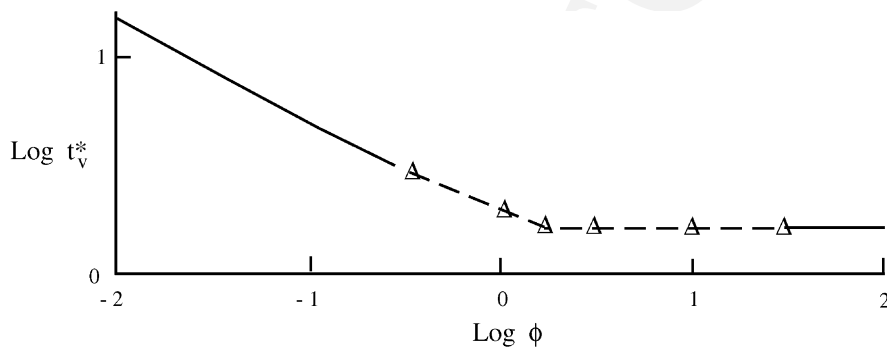


Fig. 5. A plot of the variation of dimensionless evaporation time t_v^* as a function of the relative outflow parameter ϕ . Data is taken from Table 1.

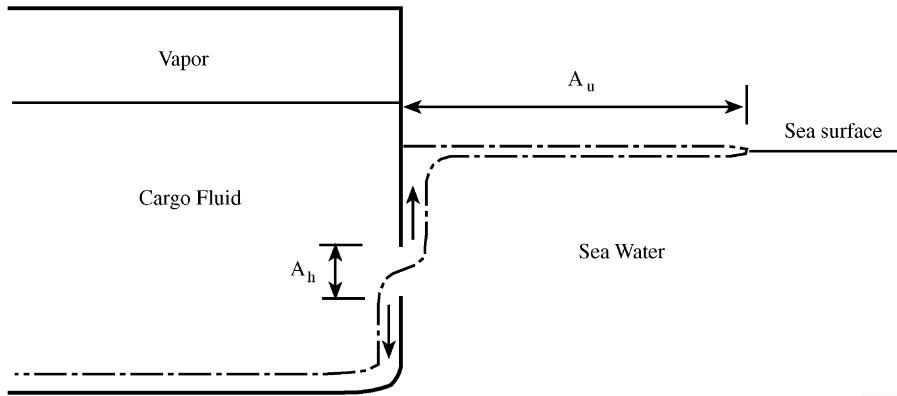


Fig. 6. A sketch of the cargo fluid outflow and sea water inflow through an underwater puncture. The dash-dot line denotes the interface between the cargo fluid and sea water.

256 10% lower, respectively, than the exact solutions of Table 1. The product $a_m^* t_v^*$ is 27% higher
 257 than the exact value of Table 1 but \bar{a}_v^* is equal to the exact value of (19).

258 2.2. Underwater punctures

259 For an underwater puncture, such as might happen in a ship collision or grounding, the
 260 effective head h driving the cargo discharge is reduced from that shown in Fig. 1 by an
 261 amount $[\Delta/(1 - \Delta)]d$, where d is the distance from the waterline to the centerline of the
 262 hole in the hull. The initial outflow is that given in Section 2, with h replaced by \hat{h} :

$$263 \quad \hat{h} \equiv h - \left(\frac{\Delta}{1 - \Delta} \right) d \quad (33)$$

264 The initial outflow will cease when $\hat{h} = 0$, with the cargo gas/liquid interface at a distance
 265 $[\Delta/(1 - \Delta)]d$ above the water line.

266 At the end of this outflow stage there is, on average, a balance in the hydrostatic pressure
 267 between the cargo fluid and the sea water external to the ship, at least at the midlevel of the
 268 puncture area. But above and below this level there is an imbalance, such that cargo fluid
 269 flows out and sea water flows in, at equal volume flow rates, as illustrated in Fig. 6. The
 270 sea water inflow displaces cargo fluid at the bottom of the cargo tank, leading to further
 271 discharge of the cargo fluid from below, rather than from above, as in the earlier discharge
 272 phase. This discharge continues until the lower part of the cargo hold is filled with sea water,
 273 up to the level of the top of the puncture. The less dense cargo fluid is decanted from the
 274 hold as sea water intrudes.

275 The volume flow rate of this discharge may be estimated. Consider first the outflow of
 276 the cargo fluid through the upper portion of the puncture. Assuming that the vertical height
 277 of the puncture is $\sqrt{A_h}$, and that a fraction f of that height and flow area is occupied
 278 by the outflow, the pressure difference driving the outflow is $\sim(\rho_w - \rho_c)gf\sqrt{A_h}$ and the

279 corresponding velocity¹ is $\sim(2[\rho_w - \rho_c]gf\sqrt{A_h}/\rho_c)^{1/2}$, leading to a volume outflow rate
 280 dV/dt of

$$282 \quad \frac{dV}{dt} \sim \left(\frac{2(\rho_w - \rho_c)gf\sqrt{A_h}}{\rho_c} \right)^{1/2} fA_h \sim \left(\frac{2(\rho_w - \rho_c)g(1-f)\sqrt{A_h}}{\rho_w} \right)^{1/2} (1-f)A_h$$

283 (34)

284 where the term on the extreme right is the equal inflow rate of the sea water. Eliminating f ,
 285 we find

$$286 \quad \frac{dV}{dt} = \gamma(2g\Delta_u A_h^{5/2})^{1/2}$$

(35)

287 where γ is an empirical constant of order unity and

$$288 \quad \Delta_u \equiv \frac{\rho_w - \rho_c}{(\rho_w^{1/3} + \rho_c^{1/3})^3}$$

(36)

289 This outflow is steady during the period of discharge because the driving pressure difference
 290 is time invariant. Consequently, after an initial transient flow as in Section 2.1.1, the pool of
 291 evaporating cargo fluid formed at the sea surface from the rising column of cargo effluent
 292 has a time-invariant area A_u given by

$$293 \quad A_u = \frac{\gamma(2g\Delta_u A_h^{5/2})^{1/2}}{w}$$

(37)

294 Nevertheless, at large enough A_u , the pool formation will become unsteady, like that for an
 295 instantaneous spill.

296 Any puncture whose vertical extent lies both above and below the vessel's waterline will
 297 completely drain the cargo fluid from the hold.

298 3. Examples

299 In this section, we consider several examples of calculations for spills from LNG and oil
 300 tankers, using typical values of the spill parameters for each type of vessel. The principal
 301 parameter variable used to express these examples is the area A_h of the puncture in the
 302 side of the vessel, which we assume to lie within the range of 1–100 m². The lower value
 303 represents the smallest hole of consequence while the higher limit is perhaps the largest to
 304 be expected in a severe collision or explosion.

305 We take as variables of interest the maximum pool area A_m and the vaporization time
 306 t_v . Expressed in terms of the dimensionless variables a_m^* and t_v^* and the dimensionless
 307 parameter ϕ (Eq. (18)), they are

$$308 \quad A_m = \left(\frac{A_h \sqrt{gh_0}}{w} \right) a_m^* = \left(\frac{\beta^2 (2\pi\Delta) gh_0^3 A_i^3}{w^2} \right)^{1/4} \frac{a_m^*}{\sqrt{\phi}}$$

(38)

¹ The interface between the cargo fluid and the sea water in the neighborhood of the puncture is unstable, leading to unsteady flow. The steady flow relations used here approximate the time-averaged flow through the puncture.

$$309 \quad t_v = \left(\frac{A_t}{A_h} \right) \sqrt{\frac{h_0}{g}} t_{v^*} = \left(\frac{A_t h_0}{\beta^2 (2\pi \Delta) g w^2} \right)^{1/4} t_{v^*} \sqrt{\phi} \quad (39)$$

310 where the dependence upon the parameter A_h is expressed through the value of ϕ in (38)
311 and (39) and the implicit dependence of a_m^* and t_v^* on ϕ (see Table 1 and Figs. 4 and 5).

312 As explained in Section 2, there is a critical value of A_h (Eq. (8)) that distinguishes
313 between the mostly quasi-steady outflow and pool formation from a small puncture and the
314 rapid unsteady outflow from a large hole. We may calculate this critical value $(A_h)_c$ from
315 Eq. (18) by using the value of $\phi_c = 1.784$ from Table 1, obtaining

$$316 \quad (A_h)_c = 0.749 \left(\frac{\beta^2 (2\pi \Delta) w^2 h_0 A_t^3}{g} \right)^{1/4} \quad (40)$$

317 The corresponding critical values of A_m and t_v are found from Eqs. (38) and (39) and Table 1
318 to be

$$319 \quad (A_m)_c = 1.071 \left[\frac{\beta^2 (2\pi \Delta) g h_0^3 A_t^3}{w^2} \right]^{1/4} \quad (41)$$

$$320 \quad (t_v)_c = 1.889 \left[\frac{A_t h_0}{\beta^2 (2\pi \Delta) g w^2} \right]^{1/4} \quad (42)$$

321 In the case of pool fires, thermal radiation can be estimated from the heat release rate of the
322 combustion of the liquid fuel. The heat release rate Q_{av} averaged over the duration of the
323 pool fire is determined from

$$324 \quad Q_{av} = \frac{(h_0 A_t) \rho_c h_c}{t_v} \quad (43)$$

325 where h_c is the fuel heating value per unit mass. For underwater punctures, the steady flow
326 heat release rate Q_u is found from Eq. (37) to be

$$327 \quad Q_u = \frac{\gamma (2g \Delta_u A_h^{5/2})^{1/2}}{w} \rho_c h_c \quad (44)$$

328 The thermal radiative flux q at a distance r from the center of the pool fire is sometimes
329 estimated as [8]:

$$330 \quad q = \frac{\eta Q}{4\pi r^2} \quad (45)$$

331 where η is the fraction of the pool heat release rate Q that is emitted as thermal radiation.
332 Eq. (45) only applies at large distances from the pool fire.

333 3.1. LNG tanker pool fire

334 LNG tankers carry a liquid cargo having a density 42% of that of sea water. The cargo
335 volume exceeds the displacement volume of the fully-loaded vessel by 30–50%, with the

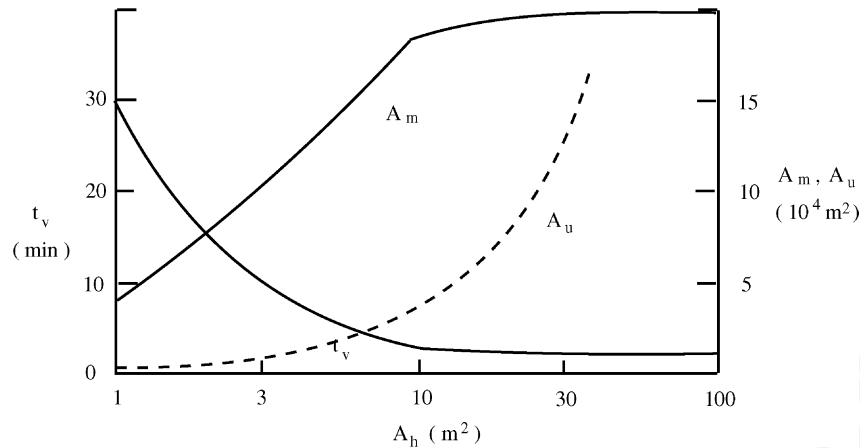


Fig. 7. Solid lines represent the maximum pool area A_m and pool fire duration t_v for a $14,300 \text{ m}^3$ spill from a single hold of an LNG tanker as a function of the puncture area A_h . Dashed line denotes the pool area A_u for an underwater puncture.

336 result that more than half the cargo volume is elevated above the vessel waterline.² If DR
 337 is the fully-loaded draft (vertical distance from the waterline to the keel), then for a typical
 338 LNG tanker the initial height h_0 of the upper surface of the cargo fluid above the waterline
 339 is about 1.1DR . The cargo surface area A_t is related to the cargo tank volume CTV by $A_t \simeq$
 340 $0.52(\text{CTV}/\text{DR})$. For an LNG tanker of $125,000 \text{ m}^3$ cargo capacity, with an 11.8 m draft and
 341 $25,000 \text{ m}^3$ cargo tank volume, $h_0 = 13 \text{ m}$ and $A_t = 1100 \text{ m}^2$. The volume of the spilled
 342 fluid, $h_0 A_t$, is $14,300 \text{ m}^3$. These values are used in subsequent calculations.

343 The LNG pool spreading and evaporation are determined by the parameters Δ , β , and
 344 w . For LNG spreading on sea water, $\Delta = 0.58$. In axisymmetric pool spreading, $\beta =$
 345 $4/\sqrt{3} = 2.31$ [2]. For confined LNG pool fires where heating from the substrate below is
 346 inconsequential, $w = 1.9 \times 10^{-4} \text{ m/s}$ [5]. For confined LNG spills on water, the maximum
 347 evaporation rate is $w = (5-7) \times 10^{-4} \text{ m/s}$; it is thought that this rate applies to unconfined
 348 spills on water [9]. Assuming that these rates should add for an unconfined pool fire on
 349 water, which is simultaneously heated from above by the pool fire and below by the warmer
 350 water, we choose $w = 8 \times 10^{-4} \text{ m/s}$.

351 A plot of the maximum pool area A_m and pool fire duration for an LNG tanker spill from
 352 a $25,000 \text{ m}^3$ hold, as a function of the puncture area A_h , is shown in Fig. 7. For A_h less than
 353 the critical value of 9.09 m^2 (see Eq. (41)), the pool area increases to $18.1 \times 10^4 \text{ m}^2$,³ while
 354 the pool fire duration t_v decreases to 3.3 min , as A_h increases to its critical value. This is the
 355 range of mostly quasi-steady flow, where the pool fire tends to consume the LNG as fast
 356 as it is disgorged onto the sea surface. For A_h greater than the critical value, there is little
 357 change in the values of A_m and t_v within the 10-fold increase in A_h shown in Fig. 7.

² Cryogenic liquid cargoes are carried in separate inner thermally insulated tanks that are supported by the ship's structure, in contrast with oil tankers where the cargo tank and ship structure are identical.

³ The maximum radius of this semicircular pool is 339 m , greater than the length of about 270 m of the LNG tanker being considered.

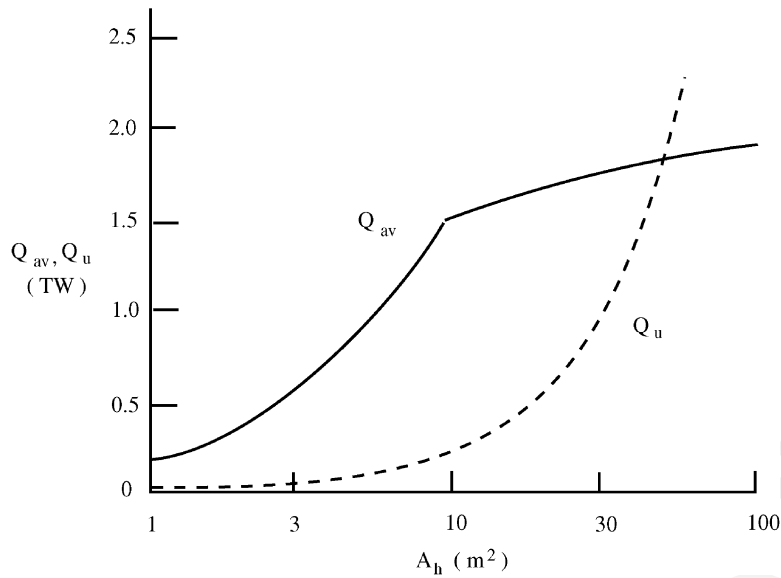


Fig. 8. Solid line represents the time-averaged heat release rate Q_{av} of a pool fire formed from a 14,300 m³ spill from a single hold of an LNG tanker as a function of the puncture area A_h . Dashed line represents the heat release rate Q_u for an underwater puncture.

358 The pool fire area A_u for an underwater puncture of area A_h is shown in Fig. 7 as a
 359 dashed line. These values are computed from Eq. (37), which assumes a balance between
 360 outflow (which is steady) and vaporization. But for the highest values of A_u shown, the high
 361 discharge rates imply a transition to unsteady pool growth and a limiting pool area as in the
 362 case of above-water discharges. The corresponding pool areas for such conditions have not
 363 been calculated.

364 The time-averaged heat release rate Q_{av} from a pool fire for this spill is plotted in Fig. 8,
 365 as a function of the puncture area A_h . Its value at the critical condition is 1.53 TW. As was
 366 the case for the other variables shown in Fig. 7, Q_{av} shows less variability for supercritical
 367 values of A_h than for subcritical ones.

368 Also plotted as a dashed line in Fig. 8 is the heat release rate Q_u for an underwater release.
 369 The limiting value for large release rates is not shown. Compared to above-water punctures,
 370 underwater ones provide smaller values of pool area and heat release rate, for a given A_h ,
 371 but nevertheless reach the above-water values at large enough A_h .

372 The distance r to a thermal radiation flux of $q = 5 \text{ kW/m}^2$, a criterion of human safety
 373 [8], may be calculated from Eq. (45) to be 1.9 km for the critical Q_{av} of an above-water
 374 release, if one assumes the lowest empirical value of $\eta = 0.15$ [8].

375 3.2. Oil tanker pool fire

376 In contrast to LNG tankers, oil product tankers have less freeboard compared with their
 377 draft, a consequence of the higher density of oil products. Also, their cargo holds are

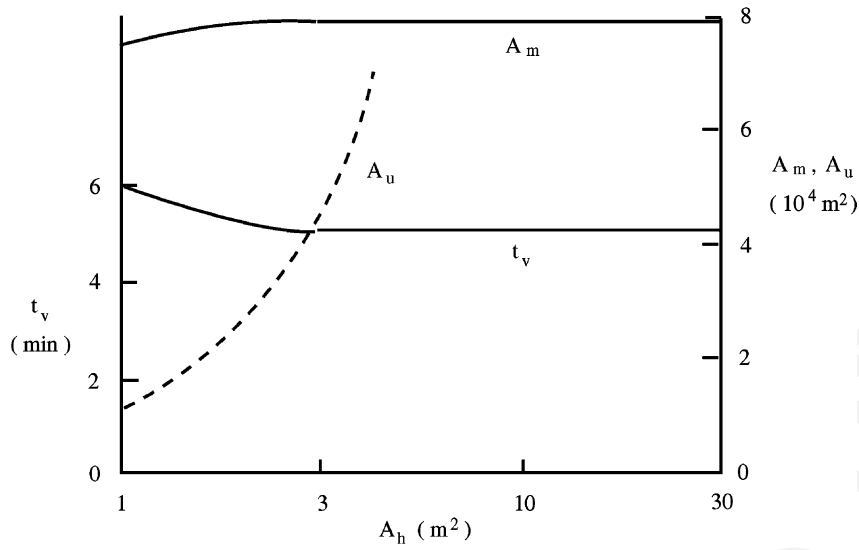


Fig. 9. Solid line denotes the maximum pool area A_m and pool fire duration t_v for a $1140 m^3$ spill of gasoline from a wing and centerline hold of an oil tanker as a function of the puncture area A_h . Dashed line denotes the pool area A_u for an underwater puncture.

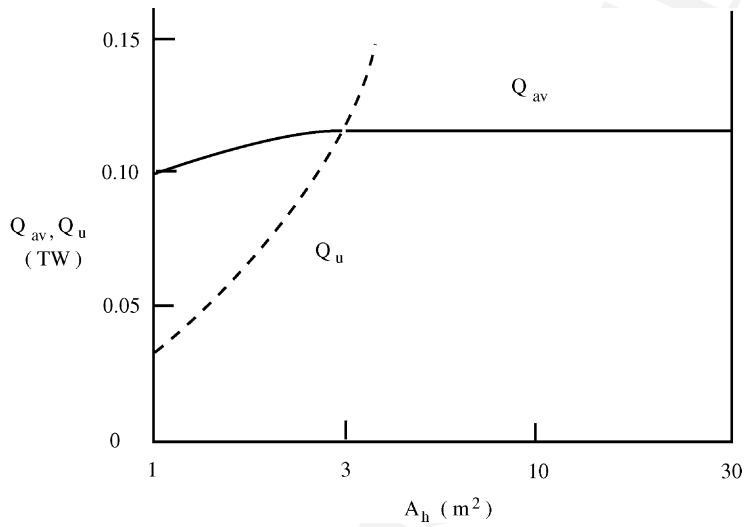


Fig. 10. Solid line denotes the time-averaged heat release rate Q_{av} of a pool fire formed from a $1140 m^3$ spill of gasoline from a wing and centerline hold of an oil tanker as a function of the puncture area A_h . Dashed line represents the heat release rate Q_u for an underwater puncture.

378 subdivided by longitudinal bulkheads into port, starboard, and centerline compartments.
379 For this example, we choose a 41,000 deadweight tonne oil tanker [10] having a combined
380 wing and center tank surface area $A_t = 285 \text{ m}^2$ and $h_0 = 4 \text{ m}$. The spill volume, $h_0 A_t =$
381 1140 m^3 , is only a quarter of the hold volume of 4450 m^3 . We assume a cargo of gasoline,
382 with density $\rho_c = 720 \text{ kg/m}^3$ and fuel heating value $h_c = 43.6 \text{ MJ/kg}$. For a gasoline pool
383 fire, we choose an evaporation rate of $w = 0.8 \times 10^{-4} \text{ m/s}$ [8].

384 The maximum pool area A_m and pool fire duration t_v for a 1140 m^3 spill of gasoline
385 from a wing and centerline hold of an oil tanker is plotted in Fig. 9 as a function of the
386 puncture area A_h . For puncture areas greater than a few square meters, the discharge time
387 is short enough that the spill may be considered instantaneous, with a maximum area of
388 $79,700 \text{ m}^2$ and a burnup time of 5.1 min. Compared with the Section 3.1 LNG spill of more
389 than 10 times this volume, the maximum pool area is about one-third as great and the fire
390 duration is 50% longer. These differences are primarily a consequence of the spill volume
391 and regression rate w . Also shown in Fig. 9 is the pool area A_u resulting from an underwater
392 puncture, for the limited hole size where a steady discharge is maintained.

393 As was done for the LNG spill of Section 3.1, we plot in Fig. 10 the time-averaged
394 heat release rate Q_{av} as a function of the puncture area A_h . For large enough A_h , Q_{av} is
395 0.116 TW , only about 8% of that for the LNG spill example. This difference reflects the
396 smaller spill volume and longer fire duration. Also shown in Fig. 10 is the heat release rate
397 Q_u for an underwater puncture.

398 4. Conclusions

399 When the cargo hold of a tanker is ruptured, the fluid cargo flows out of the hold onto
400 the surface of the ocean, in an amount and at a rate that depends upon the size and location
401 of the rupture and the dimensions and vertical placement of the hold with respect to the sea
402 surface. The outflow volume is ultimately limited by the establishment of a static equilibrium
403 between the fluid remaining in the hold and the external sea water, while the rate of outflow
404 can be estimated from inviscid gravity flow relations. The spilled fluid spreads on the sea
405 surface, eventually evaporating entirely by heating from below (in the case of cryogenic
406 fluids) and/or above if a fire is established above the pool. This dynamic outflow and pool
407 development is a time-dependent process.

408 A model of the outflow and pool development processes, expressed in dimensionless form,
409 is shown to be dependent upon a single parameter (ϕ , Eq. (18)) whose value distinguishes
410 the extreme cases of a relatively small puncture area having a slow discharge rate from its
411 inverse. In the former case, the pool fire characteristics are determined by the discharge
412 rate; in the latter case, the spill volume is determinative.

413 For cargo hold punctures that are completely or partially below the sea surface, additional
414 outflow will ensue, accompanied by sea water intrusion into the cargo hold, at rates that are
415 not yet well determined.

416 Specific examples of an LNG and oil tanker (gasoline cargo) spills show that the range
417 of credible rupture areas considered ensures that, for all but the smaller areas, the spills
418 can be considered to be instantaneous (and thereby dependent only upon the spill volume).
419 Typical LNG spills are larger in volume ($14,000$ versus 1100 m^3), their pool fires are larger

420 in area (20 versus $8 \times 10^4 \text{ m}^2$) and greater in combustion heat rate (1.9 versus 0.12 TW),
 421 and burn faster (3.3 versus 5.1 min) than oil product spills.

422 An upper limit to the maximum pool area and a lower limit to the pool fire duration
 423 may be obtained from Eqs. (38) and (39) specialized for the case of instantaneous spills
 424 ($\phi \rightarrow 0$). Using the appropriate values from Table 1 and selecting $\beta = 2.31$ as explained
 425 in Section 3.1, these limits become

$$426 \quad A_m \leq 2.58 \left(\frac{\Delta g (h_0 A_t)^3}{w^2} \right)^{1/4} \quad (46)$$

$$427 \quad t_v \geq 0.785 \left(\frac{A_t h_0}{\Delta g w^2} \right)^{1/4} \quad (47)$$

428 where $(h_0 A_t)$ is the volume of the spill and A_m is the maximum area of the semicircular
 429 pool.

430 References

- 431 [1] J.A. Fay, in: D. Hoult (Ed.), *Oil on the Sea*, Plenum Press, New York, 1965, pp. 53–63.
 432 [2] J.A. Fay, in: *Proceedings of the Joint Conference on Prevention and Control of Oil Spills*, American Petroleum
 433 Institute, Washington, DC, 1971, pp. 463–466.
 434 [3] J.A. Fay, *Comb. Sci. Tech.* 7 (1973) 47–49.
 435 [4] J.A. Fay, *Ann. Rev. Energy* 5 (1980) 89–105.
 436 [5] F.P. Lees, *Loss Prevention in the Process Industries*, 2nd Edition, Butterworth–Heinemann, Oxford, 1996,
 437 Vol. 1, pp. 15/1–333, Vol. 2, pp. 16/203–204.
 438 [6] P.K. Raj, A.S. Kalelkar, *Assessment Models in Support of the Hazard Assessment Book (CG-446-3)*, US
 439 Coast Guard, Washington, DC, 1974.
 440 [7] P.K. Raj, *Comb. Sci. Technol.* 19 (1979) 251–254.
 441 [8] K.S. Mudan, *Prog. Energy Combust. Sci.* 10 (1984) 59–80.
 442 [9] National Materials Advisory Board, *Safety Aspects of Liquefied Natural Gas in the Marine Environment*,
 443 Pub. NMAB 354, National Academy of Sciences, Washington, DC, 1980.
 444 [10] G.A.B. King, *Tanker Practice*, Stanford Maritime Ltd., London, 1971.